

# Spatiotemporal Correlations of Earthquakes

Hikaru Kawamura

*Department of Earth and Space Science, Faculty of Science, Osaka University, Toyonaka 560-0043, Japan*

Statistical properties of earthquakes are studied both by the analysis of real earthquake catalog of Japan and by numerical computer simulations of the spring-block model in both one and two dimensions. Particular attention is paid to the spatiotemporal correlations of earthquakes, *e.g.*, the recurrence-time distribution or the time evolution before and after the mainshock of seismic distribution functions, including the magnitude distribution and the spatial seismic distribution. Certain eminent features of the spatiotemporal correlations, *e.g.*, foreshocks, aftershocks, swarms and doughnut-like seismic pattern, are discussed.

## 1 Introduction

Although earthquakes are obviously complex phenomena, the basic physical picture of earthquakes seems to have been well established now: Earthquake is a stick-slip frictional instability of a fault driven by steady motions of tectonic plates [1, 2]. Although it remains to be extremely difficult at the present stage to say something really credible for each individual earthquake event, if one collects many events and take average over these events, a clear tendency often shows up there. Thus, it is sometimes possible to say something credible for the *average* or *statistical* properties of earthquakes, or more precisely, sets of earthquakes.

In this article, we wish to review some of our recent studies on the statistical properties of earthquakes. Our study of earthquakes is motivated by the following three issues.

### *Critical versus characteristic*

It has long been known empirically that certain power-laws often appear in the statistical properties of earthquakes, *e.g.*, the Gutenberg-Richter (GR) law for the magnitude distribution of earthquakes, or the Omori law for the time evolution of the frequency of aftershocks[2]. Power-law means that there is no characteristic scale in the underlying physical phenomenon. In statistical physics, one of the most widely recognized occasion of the appearance of a power-law is critical phenomena associated with a thermodynamic second-order phase transition. Indeed, inspired by this analogy, Bak and collaborators introduced the concept of the “self-organized criticality (SOC)” into earthquakes[3, 4]. According to this picture, The Earth’s crust is always in the critical state generated dynamically, and power-laws associated with statistical properties of earthquakes are regarded as realizations of the intrinsic critical nature of earthquakes. Indeed, the SOC idea gives a

natural explanation of the scale-invariant power-law behaviors frequently observed in earthquakes, including the GR law and the Omori law.

In contrast to such an SOC view of earthquakes, an opposite view has also been common in earthquake studies, a view which regards earthquakes as “characteristic”. In this view, earthquakes are supposed to possess their own characteristic scales, *e.g.*, a characteristic energy scale or a characteristic time scale.

Thus, whether an earthquake is critical or characteristic remains to be one of central issues of modern earthquake studies.

### *Possible precursory phenomena — spatiotemporal correlations of earthquakes*

In conjunction with earthquake prediction, possible precursory phenomena associated with large earthquakes have special importance. If one takes a statistical approach, a natural quantity to be examined might be spatiotemporal correlations of seismicity, *i.e.*, how earthquakes correlate in space and time. If we could identify the property in which a clear anomaly is observed preceding the large event, it might be useful for earthquake prediction. In the present article, we wish to investigate among others various types of spatiotemporal correlation functions of earthquakes.

### *The constitutive relation and the nature of stick-slip dynamics*

Since earthquakes can be regarded as a stick-slip frictional instability of a pre-existing fault, the statistical properties of earthquakes should be governed by the physical law of rock friction[1, 2]. Unfortunately, our present understanding of physics of friction is still poor. We do not have precise knowledge of the constitutive relation governing the stick-slip dynamics at earthquake faults. The difficulty lies partly in the fact that a complete microscopic theory of friction is still not available, but also in the fact that the length and

time scales relevant to earthquakes are so large that the applicability of laboratory experiments of rock friction is not necessarily clear.

A question of fundamental importance in earthquake studies might be how the properties of earthquakes depend on the constitutive relation and the material parameters characterizing earthquake faults, including the elastic properties of the crust and the constitutive parameters characterizing the friction force.

To answer this question and to get deeper insight into the physical mechanism governing the stick-slip process of earthquakes, a proper modeling of an earthquake might be an important step. In fact, earthquake models of various levels of simplifications have been proposed in geophysics and statistical physics, and their statical properties have been extensively studied mainly by means of numerical computer simulations. One of the standard model is the so-called spring-block model originally proposed by Burridge and Knopoff (BK model) [5], which we will employ in the present article. Yet, our present understanding of the question how the earthquake properties depend on the constitutive relation and the material parameters characterizing earthquake faults remains far from satisfactory.

In the present article, in order to approach the three goals mentioned above, we take two complementary approaches: In one, we perform numerical computer simulations based on the spring-block model to clarify the spatiotemporal correlations of seismic events. Both the one-dimensional (1D) BK model [6, 7] and the two-dimensional (2D) BK model [8] are studied. In the other, we analyze the earthquake catalog of Japan to examine the spatiotemporal correlations of real seismicity [9]. We then compare the results of numerical model simulation and the analysis of real earthquake catalog, hoping that such a comparison might give us useful information about the nature of earthquakes.

The following part of the article is organized as follows. In section 2, we introduce the model employed in our numerical computer simulations, and explain some the details of the simulations. We also introduce the earthquake catalog used in our analysis of real seismicity of Japan. Then, in section 3, we report on the results of our analysis of the spatiotemporal correlations of real earthquakes based on the earthquake catalog of Japan, together with the results of our numerical simulations of the 1D and 2D BK models. The statistical properties examined in this section include; (i) the magnitude distribution, (ii) the local recurrence-time distribution, (iii) the global recurrence-time

distribution, (iv) the time evolution of the spatial seismic distribution before the mainshock, (v) the time evolution of the spatial seismic distribution after the mainshock, and (vi) the time-resolved magnitude distribution before and after the mainshock. Finally, section 4 is devoted to summary and discussion of our results.

## 2 The model, the simulation and the catalog

In this section, we introduce the spring-block model which we will use in our numerical computer simulation, and explain some of the details of the simulation. We also introduce the seismic catalog of Japan which we will use in our analysis of the spatiotemporal correlations of real earthquakes. The results of our numerical computer simulations and the analysis of seismic catalog of Japan will be presented in the following section 3.

### 2.1 The spring-block model of earthquakes

The spring-block model of earthquakes was originally proposed by Burridge and Knopoff [5]. In this model, an earthquake fault is simulated by an assembly of blocks, each of which is connected via the elastic springs to the neighboring blocks and to the moving plate. All blocks are subject to the friction force, the source of the nonlinearity in the model, which eventually realizes an earthquake-like frictional instability. The model contains several parameters representing, *e.g.*, the elastic properties of the crust and the frictional properties of faults.

In the 1D BK model, the equation of motion for the  $i$ -th block can be written as

$$m\ddot{U}_i = k_p(\nu t' - U_i) + k_c(U_{i+1} - 2U_i + U_{i-1}) - \Phi_i, \quad (1)$$

where  $t'$  is the time,  $U_i$  is the displacement of the  $i$ -th block,  $\nu'$  is the loading rate representing the speed of the plate, and  $\Phi_i$  is the friction force working at the block  $i$ .

In order to make the equation dimensionless, we measure the time  $t'$  in units of the characteristic frequency  $\omega = \sqrt{k_p/m}$  and the displacement  $U_i$  in units of the length  $L = \Phi_0/k_p$ ,  $\Phi_0$  being the static friction. Then, the equation of motion can be written in the dimensionless form as

$$\ddot{u}_i = \nu t - u_i + l^2(u_{i+1} - 2u_i + u_{i-1}) - \phi_i, \quad (2)$$

where  $t = t'\omega$  is the dimensionless time,  $u_i \equiv U_i/L$  is the dimensionless displacement of the  $i$ -th block,

$l \equiv \sqrt{k_c/k_p}$  is the dimensionless stiffness parameter,  $\nu = \nu'/(L\omega)$  is the dimensionless loading rate, and  $\phi_i \equiv \Phi_i/\Phi_0$  is the dimensionless friction force working at the block  $i$ .

The form of the friction force  $\phi$  is specified by the constitutive relation. As mentioned, this part is a vitally important, yet largely ambiguous part in the proper description of earthquakes. In order for the model to exhibit a dynamical instability corresponding to an earthquake, it is essential that the friction force  $\phi$  possesses a frictional *weakening* property, *i.e.*, the friction should become weaker as the block slides.

As the simplest form of the friction force, we assume here the form used by Carlson *et al*, which represents the velocity-weakening friction force [10, 11]. Namely, the friction force  $\phi(\dot{u})$  is assumed to be a single-valued function of the velocity  $\dot{u}_i$ , *i.e.*,  $\phi_i$ , gets smaller as  $\dot{u}_i$  increases,

$$\phi(\dot{u}) = \begin{cases} (-\infty, 1], & \text{for } \dot{u}_i \leq 0, \\ \frac{1-\sigma}{1+2\alpha\dot{u}_i/(1-\sigma)}, & \text{for } \dot{u}_i > 0, \end{cases} \quad (3)$$

where its maximum value corresponding to the static friction has been normalized to unity. As noted above, this normalization condition  $\phi(\dot{u} = 0) = 1$  has been utilized to set the length unit  $L$ . The back-slip is inhibited by imposing an infinitely large friction for  $\dot{u}_i < 0$ , *i.e.*,  $\phi(\dot{u} < 0) = -\infty$ .

In this velocity-weakening constitutive relation, the friction force is characterized by the two parameters,  $\sigma$  and  $\alpha$ . The former,  $\sigma$ , represents an instantaneous drop of the friction force at the onset of the slip, while the latter,  $\alpha$ , represents the rate of the friction force getting weaker on increasing the sliding velocity. In our simulation, we regard  $\sigma$  to be small, and fix  $\sigma = 0.01$ .

It should be emphasized again that, although the above Carlson-Langer velocity-weakening friction is rather simple and has been widely used in numerical simulations, the real constitutive relation might not be so simple with features possibly different from the simplest velocity-weakening one. Indeed, there have been several other proposals for the law of rock friction, *e.g.*, the slip-weakening friction force [1, 2, 12, 13] or the rate- and state-dependent friction force [1, 2, 14, 15, 16, 17, 18]. In this article, we leave the study of these different constitutive relations to other references or to future studies, and assume the simplest velocity-weakening friction force given above.

We also assume the loading rate  $\nu$  to be infinitesimally small, and put  $\nu = 0$  during an earthquake event, a very good approximation for real faults [10, 11]. Taking this limit ensures that the interval time during successive earthquake events

can be measured in units of  $\nu^{-1}$  irrespective of particular values of  $\nu$ . Taking the  $\nu \rightarrow 0$  limit also ensures that, during an ongoing event, no other event takes place at a distant place, independently of this ongoing event.

The extension of the 1D BK model to 2D is rather straightforward. In 2D, the blocks are considered to be arranged in the form of a square array connected with the springs of the spring constant  $k_c$  [19]. We consider the isotropic and uniform case where  $k_c$  is uniform everywhere in the array independent of the spatial directions. All blocks are connected to the moving plate via the springs of the spring constant  $k_p$ , and are also subject to the velocity-weakening friction force defined above. The plate is driven along the  $x$ -direction with a constant rate  $\nu$ . It is assumed that all blocks move along the  $x$ -direction only, *i.e.*, the displacement of the block at the position  $(i_x, i_y)$  is assumed to be given by  $\vec{u}(i_x, i_y) = (u_x(i_x, i_y), 0)$ .

Since the early study by Burridge and Knopoff [5], the properties of this BK model has been studied. simulations,

Carlson, Langer and collaborators performed a pioneering study of the statistical properties of the 1D BK model quite extensively [10, 11, 19, 20, 21], with particular attention to the magnitude distribution of earthquake events. It was observed that, while smaller events persistently obeyed the GR law, *i.e.*, staying critical or near-critical, larger events exhibited a significant deviation from the GR law, being off-critical or “characteristic” [10, 19, 20, 21, 22]. Shaw, Carlson and Langer studied the same model by examining the spatiotemporal patterns of seismic events preceding large events, observing that the seismic activity accelerates as the large event approaches [23].

The BK model was also extended in several ways, *e.g.*, taking account of the effect of the viscosity [24, 25, 26], modifying the form of the friction force [24, 26], or taking account of the long-range interactions [27]. The 2D version of the BK model was also analyzed by Carlson [19] and by Myers *et al* [13].

The study of statistical properties of earthquakes was promoted in early nineties, inspired by the work by P. Bak and collaborators who emphasized the concept of “self-organized criticality (SOC)” [3, 4]. The SOC idea was developed mainly on the basis of the cellular-automaton versions of the earthquake model [3, 4, 28, 29, 30, 31, 32, 33, 34]. The statistical properties of these cellular-automaton models were also studied quite extensively, often interpreted within the SOC framework. These models apparently reproduce several fundamental features of earthquakes

such as the GR law, the Omori law of aftershocks, the existence of foreshocks, *etc.* We note that, although many of these cellular-automaton models were originally introduced to mimic the spring-block model, their statistical properties are not always identical with the original spring-block model. Furthermore, as compared with the spring-block model, the cellular-automaton models are much more simplified so that the model does not have enough room to represent various material properties of the earthquake fault in a physically appealing way. Thus, the spring-block model has an advantage over the cellular-automaton models that the dependence on the material parameters, including the constitutive and elastic properties, are more explicit.

## 2.2 The numerical simulation

As already mentioned, numerical model simulation is a quite useful tool for our purposes: First, generating huge number of events required to attain the high precision for discussing the statistical properties of earthquakes is easy to achieve in numerical simulations whereas it is often difficult to achieve in real earthquakes, especially for larger ones. Second, various material parameters characterizing earthquake faults are extremely difficult to control in real faults, whereas they are easy to control in model simulations.

We solve the equation of motion (2) by using the Runge-Kutta method of the fourth order. The width of the time discretization  $\Delta t$  is taken to be  $\Delta t\nu = 10^{-6}$ . We have checked that the statistical properties given below are unchanged even if we take the smaller  $\Delta t$ . Total number of  $10^7$  events are generated in each run, which are used to perform various averagings. In calculating the observables, initial  $10^4$  events are discarded as transients.

In order to eliminate the possible finite-size effects, the total number of blocks  $N$  are taken to be large. In 1D, we set  $N = 800$ , imposing the periodic boundary condition. The size dependence of the results was examined in Ref.[7] with varying  $N$  in the range  $800 \leq N \leq 6400$ . In 2D, we set our lattice size  $160 \times 80$  with the periodic boundary condition on the longer side, and the free boundary condition on the shorter side.

We study the properties of the model, with varying the frictional parameter  $\alpha$  and the elastic parameter  $l$ . In this article, attention is paid to the dependence on the parameter  $\alpha$ , since the parameter  $\alpha$ , which represents the extent of the frictional weakening, turns out to affect the result most significantly [7].

## 2.3 The seismic catalog of Japan

In order to compare the simulation data on the 1D and 2D BK models with the corresponding data for real earthquakes, we analyze in the following section the seismic catalog of Japan provided by Japan University Network Earthquake Catalog (JUNEC) available at <http://kea.eri.u-tokyo.ac.jp/CATALOG/junec/monthly.html>. The catalog covers earthquakes which occurred in Japan area during July 1985 and December 1998. Total of 199,446 events are recorded in the catalog. As an example, we show in Fig.1, a seismicity map of Japan generated from the JUNEC catalog, where all large earthquakes of their magnitudes greater than five, which occurred in Japan area during 1985-1998, are mapped out [35].

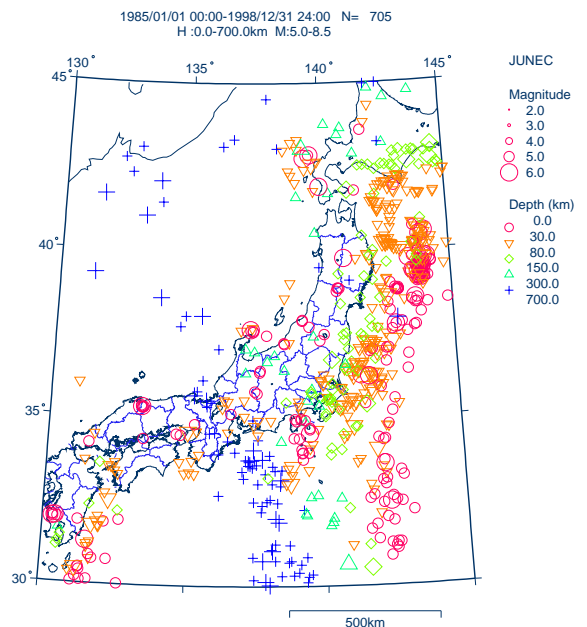


Figure 1: A seismicity map of Japan generated from the JUNEC catalog. Large earthquakes of their magnitudes greater than five, which occurred in Japan area during 1985-1998, are mapped out by using the program developed by H. Tsuruoka [35].

## 3 Statistical properties of earthquakes

In this section, we show the results of our numerical simulations of the 1D and 2D BK models, and compare them with the results of our analysis of

the seismic catalog of Japan (JUNEC catalog). We study several observables, *i.e.*, (i) the magnitude distribution, (ii) the local recurrence-time distribution, (iii) the global recurrence-time distribution, (iv) the time evolution of the spatial seismic distribution before the mainshock, (v) the time evolution of the spatial seismic distribution after the mainshock, and (vi) the time-resolved magnitude distribution before and after the mainshock. We show these results consecutively below.

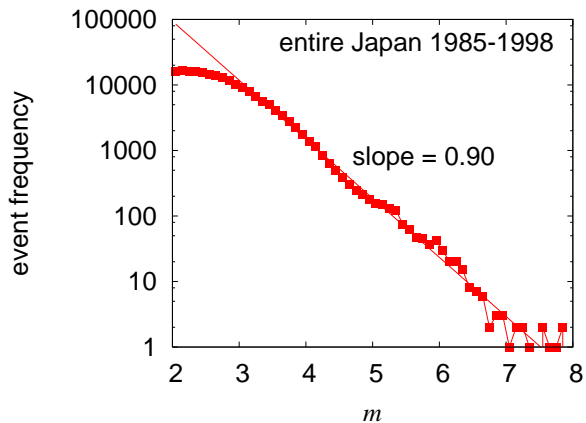


Figure 2: The magnitude distribution of earthquakes in Japan generated from the JUNEC catalog. The data for  $m > 3$  lie on a straight line with the GR exponent  $b \simeq 0.9$ .

### 3.1 The magnitude distribution

In Fig.2 we show the magnitude distribution  $R(m)$  of earthquakes of Japan generated from the JUNEC catalog, where  $R(m)dm$  represents the rate of events with their magnitudes in the range  $[m, m + dm]$ . The data lie on a straight line fairly well for  $m > 3$ , obeying the GR law. The slope of the straight line gives the power-law exponent about  $b \simeq 0.9$ .

In Fig.3(a), we show the magnitude distribution  $R(\mu)$  of earthquakes calculated from our numerical simulation of the 1D BK model. The parameter  $\alpha$  is varied in the range  $0.25 \leq \alpha \leq 10$ , while the elastic parameter  $l$  is fixed to  $l = 3$ .

In the BK model, the magnitude of an event,  $\mu$ , is defined as the logarithm of the moment  $M_0$ , *i.e.*,

$$\mu = \ln M_0, \quad M_0 = \sum_i \Delta u_i, \quad (4)$$

where  $\Delta u_i$  is the total displacement of the  $i$ -th block during a given event and the sum is taken over all blocks involved in the event [10]. It should be noticed that the absolute numerics of the magnitude value of the BK model  $\mu$  has no direct

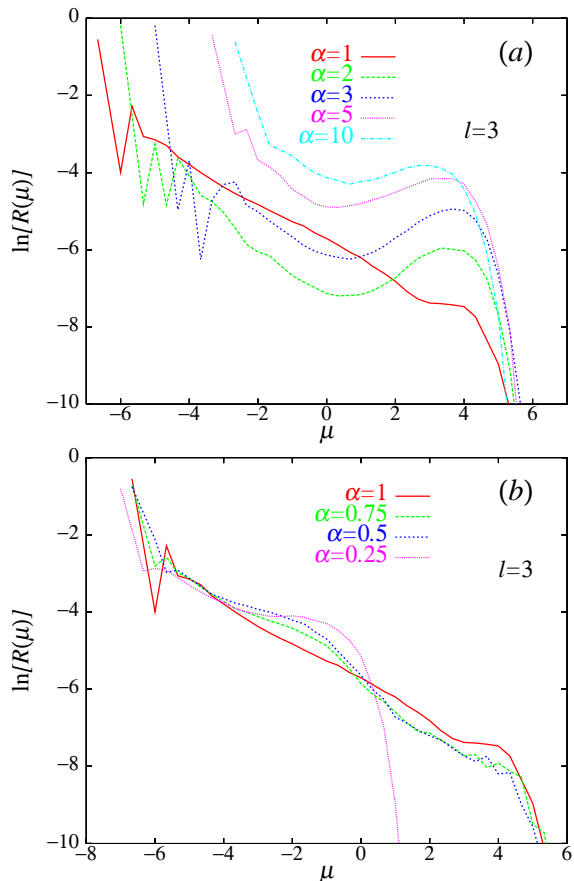


Figure 3: The magnitude distribution of seismic events calculated for the 1D BK model, for the range of larger  $\alpha \geq 1$  (a), and for the range of smaller  $\alpha \leq 1$  (b).

quantitative correspondence to the magnitude  $m$  of real earthquakes.

As can be seen from Fig.3, the form of the calculated magnitude distribution depends on the  $\alpha$ -value considerably. The data for  $\alpha = 1$  lie on a straight line fairly well, apparently satisfying the GR law. The value of the exponent  $B$  describing the GR-like power-law behavior,  $\propto 10^{-B}$ , is estimated to be  $B \simeq 0.50$  corresponding to  $b \simeq 0.75$ , which is slightly smaller than the  $b$ -value observed for the JUNEC catalog  $b \simeq 0.9$ . Remember the relation  $b = \frac{3}{2}B$ .

On the other hand, the data for larger  $\alpha$ , *i.e.*, the ones for  $\alpha \geq 2$  deviate from the GR law at larger magnitudes, exhibiting a pronounced peak structure, while the power-law feature still remains for smaller magnitudes. These features of the magnitude distribution are consistent with the earlier observation of Carlson and Langer [10, 20]. It means that, while smaller events exhibit self-similar critical properties, larger events tend to exhibit off-critical or characteristic properties, much

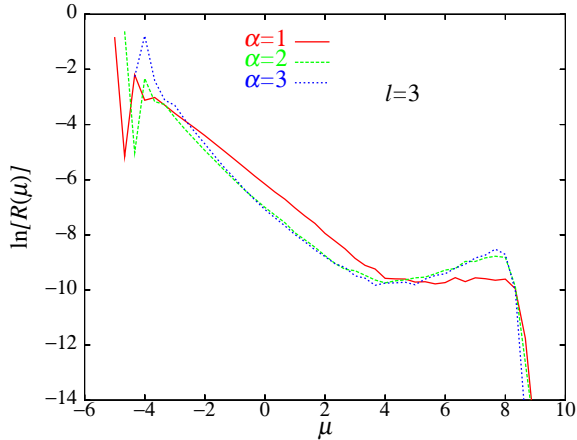


Figure 4: The magnitude distribution of seismic events calculated for the 2D BK model.

more so as the velocity-weakening tendency of the friction is increased. The observed peak structure gives us a criterion to distinguish large and small events. Below, we regard events with their magnitudes  $\mu$  greater than  $\mu_c = 3$  as large events of the 1D BK model,  $\mu_c = 3$  being close to the peak position of the magnitude distribution of Fig.3(a). In an earthquake with  $\mu = 3$ , the mean number of moving blocks are about 76 ( $\alpha = 1$ ) and 60 ( $\alpha = 2, 3$ ).

As can be seen from Fig.3(b), the data at smaller  $\alpha < 1$  exhibit considerably different behaviors from those for  $\alpha > 1$ . Large events are suppressed here. For  $\alpha = 0.25$ , in particular, all events consist almost exclusively of small events only. This result might be consistent with the earlier observation which suggested that the smaller value of  $\alpha < 1$  tended to cause a creeping-like behavior without a large event [20]. In particular, Vasconcelos showed that a single block system exhibited a “first-order transition” at  $\alpha = 0.5$  from a stick-slip to a creep [36], whereas this discontinuous transition becomes apparently continuous in many-block system [37, 38]. Since we are mostly interested in large seismic events here, we concentrate in the following on the parameter range  $\alpha \geq 1$ . In contrast to the parameter  $\alpha$ , the magnitude distribution turns out to be less sensitive to the stiffness parameter  $l$ . Further details of the  $l$ -dependence is given in Ref.[7].

In Fig.4, we show the magnitude distribution  $R(\mu)$  of the 2D BK model with varying the  $\alpha$  value. At larger magnitudes, a deviation from the GR law is observed for any value of  $\alpha$ , *i.e.*, the calculated magnitude distribution exhibits a peak structure at larger magnitude irrespective of the  $\alpha$ -value, suggesting that larger earthquakes tend to be characteristic. From the observed peak

structure, we regard events with their magnitudes  $\mu$  greater than  $\mu_c = 5$  as large events of the 2D BK model.

While the BK model tends to reproduce the GR law for earthquakes of smaller magnitudes, its relevance to the GR law observed in real seismicity is not entirely clear. It has been suggested that the GR  $b$ -value might be related to the fractal dimension of the fault interface [39, 40, 41]. More recently, Chakrabarti and collaborators proposed an earthquake model in which the magnitude distribution of earthquakes is related to the contact area distribution between the two fractal surfaces of the plates [42]. In these approaches, the intrinsic nonuniformity at earthquake faults plays an essential role in realizing the GR law and the critical nature of earthquakes. Whether this is really true, as well as its possible relation to the BK model where the nonuniformity is apparently absent, or at least not explicit, needs to be examined further.

### 3.2 The local recurrence-time distribution

A question of general interest may be how large earthquakes repeat in time, do they occur near periodically or irregularly? One may ask this question either locally, *i.e.*, for a given finite area on the fault, or globally, *i.e.*, for an entire fault system. The picture of characteristic earthquake presumes the existence of a characteristic recurrence time. In this case, the distribution of the recurrence time of large earthquakes,  $T$ , is expected to exhibit a peak structure at such a characteristic time scale. If the SOC concept applies to large earthquakes, by contrast, such a peak structure would not show up.

In the upper panel of Fig.5, we show the distribution of the local recurrence time  $T$  of large earthquakes of Japan with  $m \geq m_c = 4$ , calculated from the JUNEK catalog. In defining the recurrence time locally, the subsequent large event is counted when a large event with  $m \geq m_c = 4$  occurs with its epicenter lying within a circle of radius 30 km centered at the epicenter of the previous large event. The mean recurrence time  $\bar{T}$  is then estimated to be 148 days. In the middle and lower panels of Figs.5, the same data are re-plotted on a double-logarithmic scale [middle panel], and on a semi-logarithmic scale [lower panel], with the magnitude threshold  $m_c = 3, 4$  and 5. One sees from these figures that the local recurrence-time distribution exhibits power-law-like critical features at shorter times, which seems to cross over to a faster exponential-like decay at longer times. The time range in which the data obey a power-

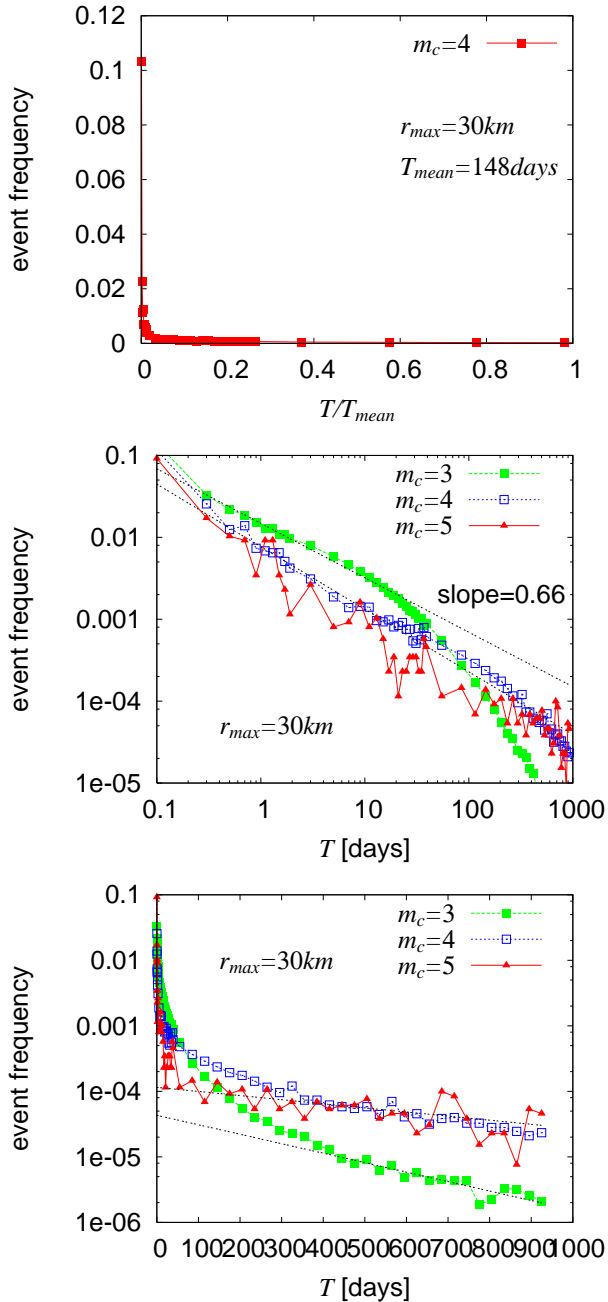


Figure 5: The local recurrence-time distribution of large earthquakes in Japan generated from the JUNEK catalog. The distribution is given on a bare scale for large earthquakes with  $m_c = 4$  [upper figure], on a logarithmic scale with  $m_c = 3, 4$  and  $5$  [middle figure], and on a semi-logarithmic scale with  $m_c = 3, 4$  and  $5$  [lower figure].

law tends to get longer for larger earthquakes. The power-law exponent estimated for earthquakes of  $m_c = 5$  in the time range  $T < 1000$  days is about  $\frac{2}{3}$ . This value is a bit smaller than the standard Omori exponent  $\simeq 1$ .

In the upper panel of Fig.6, we show the distribution of the local recurrence time  $T$  of large earthquakes with  $\mu \geq \mu_c = 3$ , calculated for the 1D BK model. In the insets, the same data including the tail part are re-plotted on a semi-logarithmic scale. In defining the recurrence time locally in the BK model, the subsequent large event is counted when a large event occurs with its epicenter in the region within 30 blocks from the epicenter of the previous large event. The mean recurrence time  $\bar{T}$  is then estimated to be  $\bar{T}\nu = 1.47, 1.12,$  and  $1.13$  for  $\alpha = 1, 2$  and  $3,$  respectively.

As can be seen from Fig.6, the tail of the distribution is exponential at longer  $T > \bar{T}$  for all values of  $\alpha$ , while the form of the distribution at shorter  $T < \bar{T}$  is non-exponential and differs between for  $\alpha = 1$  and for  $\alpha = 2$  and  $3$ . For  $\alpha = 2$  and  $3$ , the distribution has an eminent peak at around  $\bar{T}\nu \simeq 0.5$ , not far from the mean recurrence time. This means the existence of a characteristic recurrence time, suggesting the near-periodic recurrence of large events. This characteristic behavior is in sharp contrast to the critical behavior without any peak structure observed in the JUNEK data. It should also be mentioned, however, that there were reports in the literature of a near-periodic recurrence of large events at several real faults [2, 43].

For  $\alpha = 1$ , by contrast, the peak located close to the mean  $\bar{T}$  is hardly discernible. Instead, the distribution has a pronounced peak at a shorter time  $\bar{T}\nu \simeq 0.10$ , just after the previous large event. In other words, large events for  $\alpha = 1$  tend to occur as “twins”. This has also been confirmed by our analysis of the time record of large events. In fact, as shown in Ref.[7], a large event for the case of  $\alpha = 1$  often occurs as a “unilateral earthquake” where the rupture propagates only in one direction, hardly propagating in the other direction. When a large earthquake occurs in the form of such a unilateral earthquake, further loading due to the plate motion tends to trigger the subsequent large event in the opposite direction, causing a twin-like event. This naturally explains the small- $T$  peak observed in Figs.6 for  $\alpha = 1$ .

In the lower panel of Fig.6, the local recurrence-time distribution of large events is shown for the cases of  $\alpha = 1$ , with varying the magnitude threshold as  $\mu_c = 2, 3$  and  $4$ . As can be seen from this figure, the form of the distribution for  $\alpha = 1$  largely changes with the threshold

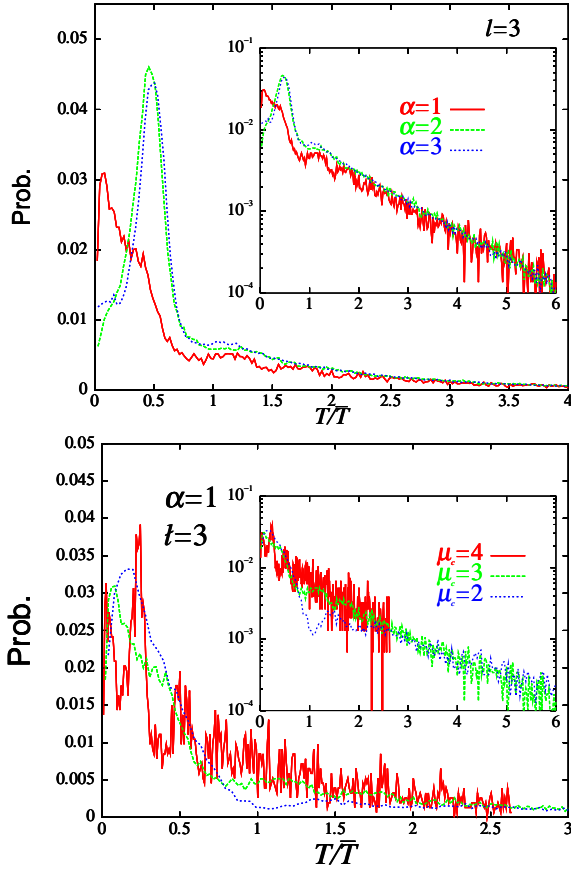


Figure 6: The local recurrence-time distribution of large events of the 1D BK model. In the upper figure, the distribution is given for  $\alpha = 1, 2$  and  $3$  with fixing  $\mu_c = 3$ , whereas, in the lower figure, the distribution is given with varying the magnitude threshold as  $\mu_c = 2, 3$  and  $4$  with fixing  $\alpha = 1$ .

value  $\mu_c$ . Interestingly, in the case of  $\mu_c = 4$ , the distribution has *two* distinct peaks, one corresponding to the twin-like event and the other to the near-periodic event. Thus, even in the case of  $\alpha = 1$  where the critical features are apparently dominant for smaller thresholds  $\mu_c = 2$  and  $3$ , features of a characteristic earthquake becomes increasingly eminent when one looks at very large events.

In Fig.7, the local recurrence-time distribution is shown for the 2D BK model. In defining the recurrence time locally in the 2D BK model, a subsequent large event is counted when a large event occurs with its epicenter lying within a circle of its radius 5 blocks centered at the epicenter of the previous large event. The mean recurrence time  $\bar{T}$  is then estimated to be  $\bar{T}\nu = 1.47, 1.12,$  and  $1.13$  for  $\alpha = 1, 2$  and  $3$ , respectively. The behavior of the 2D model is similar to the 1D model, with enhanced characteristic features. The peak struc-

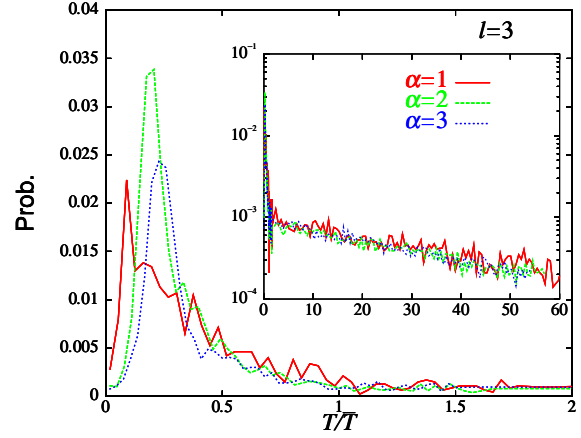


Figure 7: The local recurrence-time distribution of large events of  $\mu > \mu_c = 5$  of the 2D BK model.

ture of the distribution is very prominent even for  $\alpha = 1$ .

### 3.3 The global recurrence-time distribution

In this subsection, we examine the global recurrence-time distribution. By the word “global”, we consider the situation where the region in which one identifies the next event is sufficiently wide, much wider than the typical size of the rupture zone of large events.

From the JUNEC catalog, we construct in the upper panel of Fig.8 such *global* recurrence-time distribution for entire Japan for large earthquakes with  $m_c = 4$ . The mean recurrence time  $\bar{T}$  is then estimated to be 0.73 days. In the middle and lower panels of Figs.8, the same data are re-plotted on a double-logarithmic scale [middle], and on a semi-logarithmic scale [lower], with the magnitude threshold  $m_c = 3, 4$  and  $5$ . One sees from these figures that the global recurrence-time distribution of the JUNEC data is very much similar to the corresponding local recurrence-time distribution shown in Figs.5: It exhibits power-law-like critical features at shorter times, which crosses over to a faster exponential-like decay at longer times. The time range in which the data obey a power-law gets longer for larger earthquakes. The exponent describing the power-law regime is roughly about  $\frac{2}{3}$ , which is not far from the corresponding exponent of the local recurrence-time distribution.

Fig.9 exhibits the *global* recurrence-time distribution of large events with  $\mu_c = 3$  calculated for the 1D BK model. As can clearly be seen from the figure, in the BK model, the form of the distribution takes a different form from the local one: The peak structure seen in the local distribution



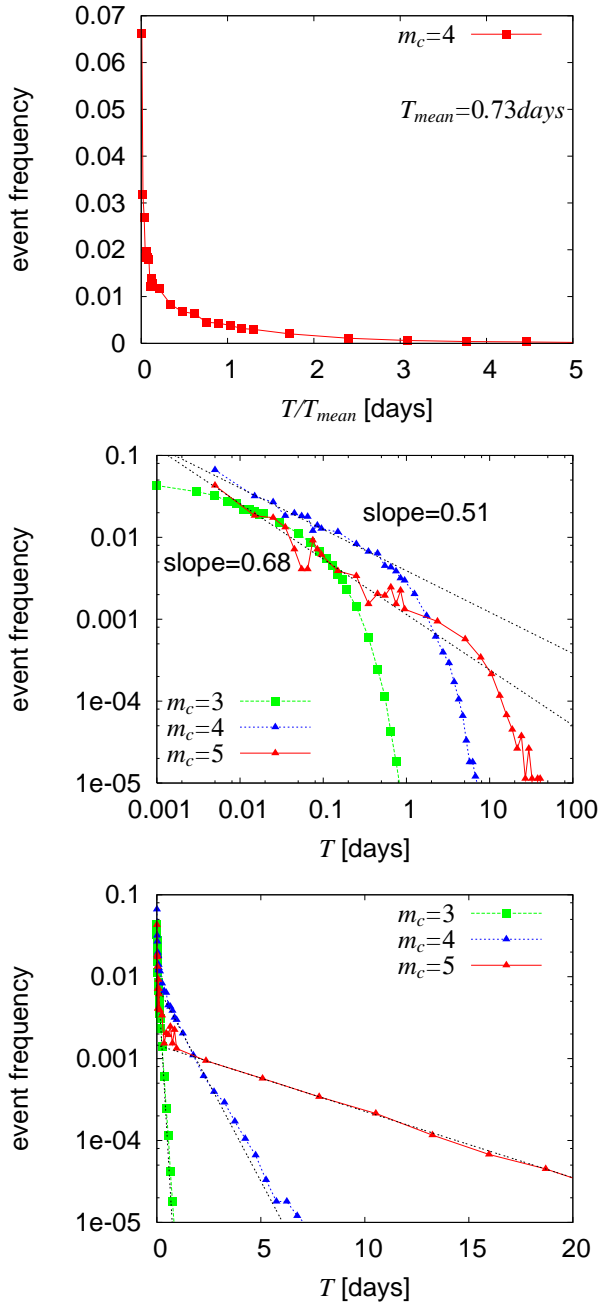


Figure 8: The global recurrence-time distribution of large earthquakes in entire Japan generated from the JUNEK catalog. The distribution is given on a bare scale for large earthquakes with  $m_c = 4$  [upper figure], on a double-logarithmic scale with varying  $m_c = 3, 4$  and  $5$  [middle figure], and on a semi-logarithmic scale with varying  $m_c = 3, 4$  and  $5$  [lower figure].

no longer exists here. Furthermore, the form of the distribution tail at larger  $T$  is not a simple exponential, faster than exponential: See a curvature of the data in the inset of Fig.9. These features of the global recurrence-time distribution turn out to be rather robust against the change of the parameter values such as  $\alpha$  and  $l$ , as long as the system size is taken to be sufficiently large.

The observation that the local and the global recurrence-time distributions exhibit mutually different behaviors means that the form of the distribution depends on the length scale of measurements. Such scale-dependent features of the recurrence-time distribution of the BK model are in apparent contrast with the scale-invariant power-law features of the recurrence-time distributions observed in the JUNEK data shown in Figs.5 and 8, and the ones reported for some of real faults [44, 45]. We note that essentially the same behavior as the one of the 1D BK model is also observed in the 2D BK model (the data not shown here).

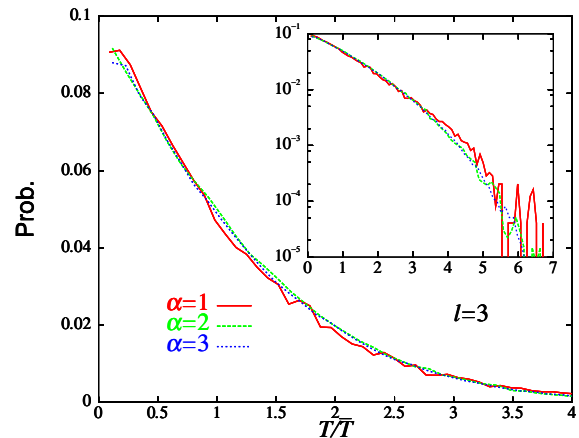


Figure 9: The global recurrence-time distribution of large events of the 1D BK model. The distribution is given for  $\alpha = 1, 2$  and  $3$  with fixing the magnitude threshold  $\mu_c = 3$ .

### 3.4 Spatiotemporal seismic correlations before the mainshock

In this subsection, we study the spatiotemporal correlations of earthquake events before the mainshock.

We begin with the JUNEK catalog. First, we define somewhat arbitrarily the mainshock as an event whose magnitude  $m$  is greater than  $m_c = 5$ , and pay attention to the frequency of earthquake events preceding the mainshock, particularly its time and distance dependence. Both the time  $t$

and the distance  $r$  are measured relative to the time and the position of the subsequent mainshock. The distance between the two events is measured here as the distance between their epicenters. The event frequency is normalized by the factor  $r$  associated with the area element of the polar coordinate.

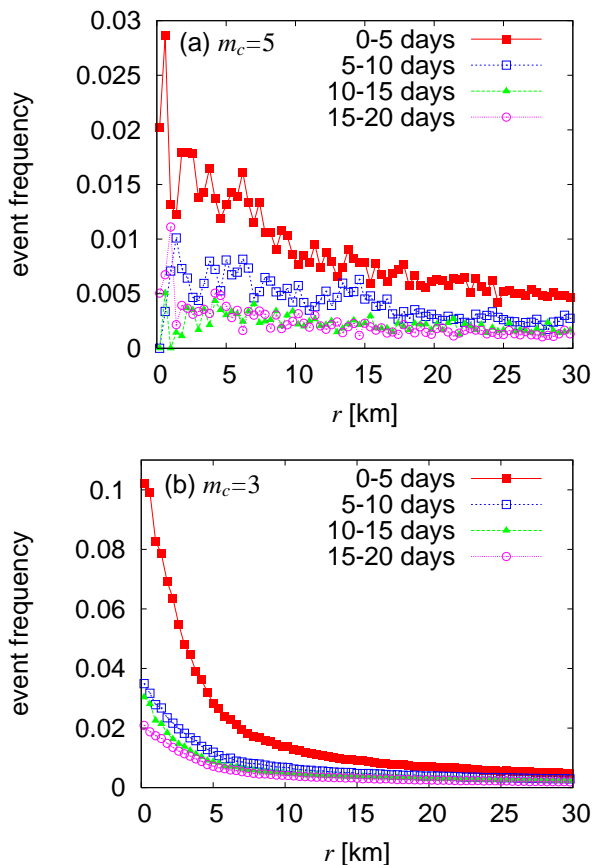


Figure 10: The time evolution of the event frequency of arbitrary magnitude preceding the mainshock, plotted as a function of the distance from the epicenter of the upcoming mainshock. The magnitude threshold for the mainshock is  $m_c = 5$  (a) and  $m_c = 3$  (b). The data are generated from the JUNEK catalog, while the contribution from the two special regions, *i.e.*, the Izu region and the Ebino region, has been omitted from the data: See the text for further details.

Fig.10 exhibits the event frequency plotted as a function of  $r$ , the distance from the upcoming mainshock, for four time periods preceding the mainshock each containing five days. The data show the time evolution of the spatial pattern of event number irrespective of its magnitude, which occur within 30 km from the epicenter of the upcoming mainshock and during the last 20 days toward the mainshock. The data have been averaged over the mainshocks contained in

the data set taken over entire Japan, but *omitting the contributions of the two special narrow regions, i.e., Izu and Ebino*. In these two regions, active earthquake “swarms” occurred during the period, which lead to significantly different behavior in the spatiotemporal correlations (we return to this point later in this subsection). In the data set, total of 990 mainshocks are included, each mainshock accompanying about 8.7 preceding events on average in the time/space range shown in the figure. As can clearly be seen from Fig.10(a), there is a tendency that the seismic activity accelerates as the mainshock approaches, and this tendency is more pronounced in a closer vicinity of the epicenter of the upcoming mainshock. The data demonstrate that the mainshock accompanies *foreshocks*, at least in the statistical sense.

It should be emphasized here that the evidence of foreshock activity becomes clear only after averaging over a large number of mainshocks. Note that, in the time/space region of interest, each single mainshock accompanies on average less than ten foreshocks only, a too small number to say anything definite.

One may wonder if certain qualitative features of the spatiotemporal correlations shown in Fig.10(a) might change depending on the region, the depth and the magnitude-threshold of the mainshock. Examination of the JUNEK data, however, reveals that the qualitative features of Fig.10(a) are rather robust against these parameters. The average number of foreshocks depends somewhat on each region in Japan: For example, the mean numbers of foreshocks in the space/time region of Fig.10(a) are 9.4 for the northern part of Japan ( $40^\circ\text{N}$ - latitude), 14.7 for the middle part ( $36^\circ\text{N}$ - $40^\circ\text{N}$ ) and 3.6 for the southern part ( $-36^\circ\text{N}$ ). Nevertheless, the qualitative features of the spatiotemporal correlations turn out to be more or less common.

In Fig.10(b), we show the similar spatiotemporal seismic correlations as in Fig.10(a), but now reducing the magnitude threshold of the mainshock from  $m_c = 5$  to  $m_c = 3$ . By this definition, the total number of mainshocks is increased to 53,835 so that the better statistics is expected. Indeed, the data shown in Fig.10(b) are far less erratic than those in Fig.10(a), reflecting the improvement of the statistics. Nevertheless, the qualitative features remain almost the same as in Fig.10(a).

In order to clarify the relation with the inverse Omori law which describes the time evolution of the frequency of foreshocks, we show in Fig.11 the time dependence of the frequency of foreshocks before the mainshock on a double-logarithmic scale: In the upper panel, the data with the distance range  $r_{max} = 30$  km are shown with varying the

magnitude threshold as  $m_c = 3, 4$  and  $5$ , while in the lower panel, the data with  $m_c = 5$  are shown with varying the distance range as  $r_{max} = 5, 30$  and  $300$  km. Except for the case of very large distance range  $r_{max} = 300$  km, the inverse Omori exponent comes around  $0.5$ .

Now, we wish to turn to the spatiotemporal correlations in the two special regions, the contribution of which have intentionally been omitted in our analysis of Figs.10 and 11. In fact, these special regions are associated with “swarms”. If there occurs an earthquake swarm which contains in itself a few large events which can be regarded as mainshocks, they make a significant contribution to the above spatiotemporal correlations because a huge number of small events are contained in swarms. The two swarms we discarded in our analysis of Figs.10 and 11 are, (i) the Izu earthquake swarm, and (ii) the Ebino earthquake swarm (Ebino is located close to the Kirishima volcanoes in southern Kyusyu). Indeed, if the contribution of these two swarm regions were not separated in our analysis of Figs.10 and 11, the resulting distribution function would look considerably different.

In Figs.12, we show the the spatiotemporal seismic correlations associated with mainshocks with  $m_c = 5$  in the Izu swarm region [34.8°N-35.1°N latitude; 139.0°E-139.5°E longitude] (a), and in the Ebino swarm region [31.8°N-32.0°N; 130.2°E-130.6°E] (b), respectively. The total numbers of mainshocks are 4 (Izu) and 6 (Ebino) here. In either case, the average number of foreshocks per mainshock is very large. In the case of Izu, it is about 256 within the range of 30km and 20 days from the mainshock, which is an order of magnitude larger than the number associated with swarm-unrelated mainshocks.

As can immediately be seen from Figs.12, the spatiotemporal pattern of these regions are quite different from the one in other regions shown in Figs.10, which suggests that the property of swarm-related earthquakes might differ qualitatively from that of swarm-unrelated earthquakes. For example, foreshocks in the Izu swarm region suddenly accelerate on the onset time of about a week, with the center of activity about 5 km away from the mainshock position, the associated spatial correlation function exhibiting a pronounced peak at about  $r \simeq 5$  km. This seismic pattern is not dissimilar to the doughnut-like seismic pattern discussed by Mogi as occurring preceding the mainshock (Mogi doughnut) [46]. However, since the doughnut-like seismic pattern as observed in Figs.12 is not observed in our analysis of more generic case of the wider region, at least in a statistically significant manner, it is likely to be related

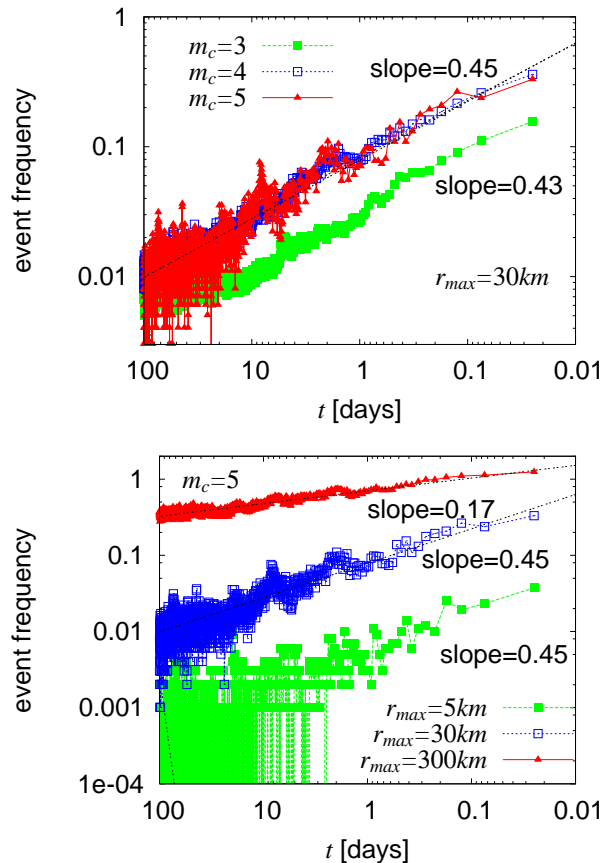


Figure 11: The frequency of seismic events of arbitrary magnitude preceding the mainshock, plotted versus the time until the mainshock on a double-logarithmic scale. The data are generated from the JUNE catalog, where the contribution from the two special regions, *i.e.*, the Izu region and the Ebino region, has been omitted: See the text for further details. In the upper figure, the magnitude threshold of the mainshock is varied as  $m_c = 3, 4$  and  $5$  with fixing the distance range of observation  $r_{max} = 30$  km, whereas, in the lower figure, the distance range of observation is varied as  $r_{max} = 5, 30$  and  $300$  km with fixing the magnitude threshold  $m_c = 5$ .

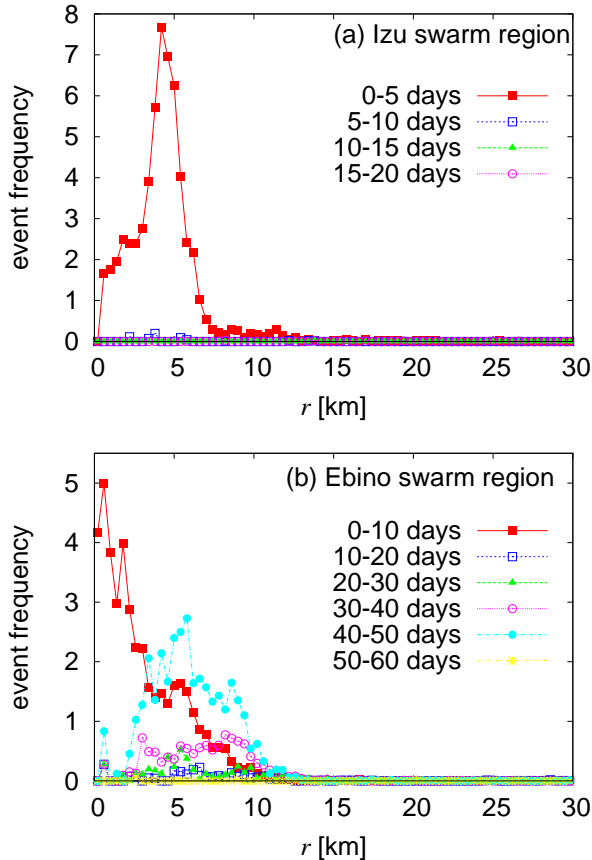


Figure 12: The time evolution of the event frequency of arbitrary magnitude preceding the mainshock, plotted versus the distance from the epicenter of the upcoming mainshock. The data are generated from the JUNEK catalog, for the Izu earthquake swarm region [34.8°N-35.1°N latitude; 139.0°E-139.5°E longitude] (a), and for the Ebino earthquake swarm region [31.8°N-32.0°N; 130.2°E-130.6°E] (b), both during the period 1985-1998. The magnitude threshold of the mainshock is  $m > m_c = 5$

to the specialty of Izu (and Ebino) region. Swarm activity is considered to be related to the activity of underground magma or water. Hence, some of the statistical properties of swarm-related earthquakes might be better discriminated from those of more general swarm-unrelated earthquakes.

We examine next the corresponding spatiotemporal correlations of the BK model. In the BK model, the distance from the epicenter is measured in units of blocks. Fig.13 represents the time evolution of the spatial distribution of seismicity before the mainshock with  $\mu > \mu_c = 3$  for  $\alpha = 1$ . Very much similar behaviors are observed for other values of  $\alpha$ . Similarly to the JUNEK data, preceding the mainshock, there is a tendency of the frequency of smaller events to be enhanced at and

around the epicenter of the upcoming mainshock. This was also observed previously by Shaw *et al* [23].

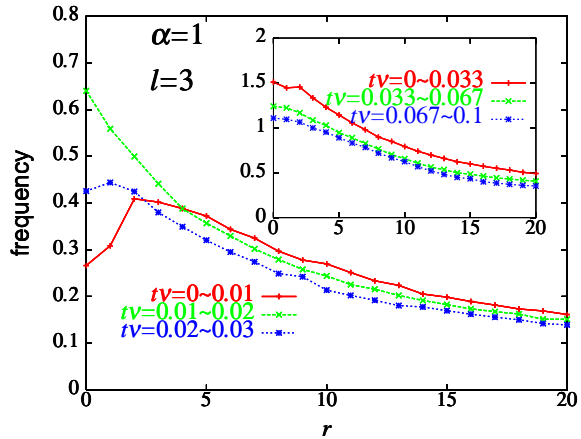


Figure 13: The time evolution of the spatial seismic distribution function before the mainshock of  $\mu > \mu_c = 3$ , calculated for the 1D BK model. The inset represents a similar plot with longer time intervals.

Interestingly, however, as the mainshock becomes imminent, the frequency of smaller events is suppressed in a close vicinity of the epicenter of the upcoming mainshock, though it continues to be enhanced in the surroundings (Mogi doughnut) [2, 46]. We note that the quiescence observed here occurs only in a close vicinity of the epicenter of the mainshock, within one or two blocks from the epicenter, and only at a time close to the mainshock. The time scale for the appearance of the doughnuts-like quiescence depends on the  $\alpha$ -value: The time scale of the onset of the doughnut-like quiescence tends to be longer for larger  $\alpha$ . It is not clear at the present stage whether the doughnut-like quiescence as observed here in the BK model has any relevance to the one observed in Figs.12 for certain earthquake swarms.

As was discussed in detail in Ref.[7], in the BK model, the size of the “hole” of the doughnut-like quiescence as well as its onset time scale have no correlation with the magnitude of the upcoming event. In other words, the doughnut-like quiescence is not peculiar to large events in the present model. This means that, by monitoring the onset of the “hole” in the seismic pattern of the BK model, one can certainly deduce the time and the position of the upcoming event, but unfortunately, cannot tell about its magnitude. Yet, one might get some information about the magnitude of the upcoming event, not from the size and the onset time of the “hole”, but from the size of the “ring” surrounding the “hole”. Thus, we show in Figs.14 the spatial correlation functions before the main-

shock in the time range  $0 \leq t\nu \leq 0.001$  for the case of  $\alpha = 2$ , with varying the magnitude range of the upcoming event. In the figure, the direction in which the rupture propagates farther in the upcoming event is always taken to be the positive direction  $r > 0$ , whereas the direction in which the rupture propagates less is taken to be the negative direction  $r < 0$ . As can be seen from the figure, although the size of the “hole” around the origin  $r = 0$  has no correlation with the magnitude of the upcoming event as mentioned above, the size of the region of the active seismicity surrounding this “hole” is well correlated with the size and the direction of the rupture of the upcoming event. This coincidence might enable one to deduce the position and the size of the upcoming event by monitoring the pattern of foreshocks, although it is still difficult to give a pinpoint prediction of the time of the upcoming mainshock. We note that such a correlation between the size of the seismically active region and the magnitude of the upcoming event was observed in the BK model in Ref.[47], and was examined in real earthquake data as well [48].

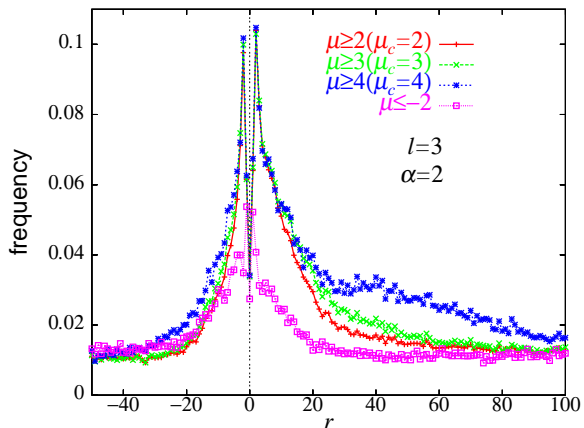


Figure 14: The frequency of seismic events preceding the events of various magnitude range plotted versus  $r$ , the distance from the epicenter of the upcoming mainshock. The curves correspond to the large events of  $\mu > \mu_c = 2, 3$  and  $4$ , and to the smaller events of  $\mu < -2$ . The direction in which the rupture propagates farther in the upcoming mainshock is always taken to be the positive direction  $r > 0$ , whereas the direction in which the rupture propagates less is taken to be the negative direction  $r < 0$ . The parameters are taken to be  $\alpha = 2$  and  $l = 3$ , the time range being  $0 \leq t\nu \leq 0.001$  before the mainshock.

As shown in Fig.15, a very much similar behavior including the doughnut-like quiescence is observed also in the 2D BK model. Note that the event frequency has been normalized here by the

measure factor  $r$  associated with the area element of the polar coordinate. The time scale of the onset of the doughnut-like quiescence seems to be longer in 2D than in 1D.

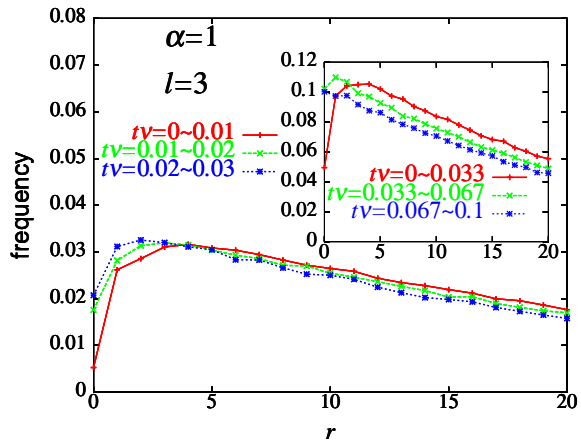


Figure 15: The time evolution of the spatial seismic distribution function before the mainshock of  $\mu > \mu_c = 5$ , calculated for the 2D BK model. The inset represents a similar plot with longer time intervals.

### 3.5 Spatiotemporal seismic correlations after the mainshock

In this subsection, we examine the spatiotemporal correlations of earthquake events *after* the mainshock. The time evolution of the spatial seismic pattern calculated from the JUNEC catalog are shown in Fig.16, with the magnitude threshold for the mainshock  $m_c = 5$  (a), and  $m_c = 3$  (b). As can be seen from these figures, aftershock activity is clearly observed. The rate of the aftershock activity is highest just at the epicenter of the mainshock, not in the surroundings. It is sometimes mentioned in the literature that the aftershock activity is highest near the edge of the rupture zone of the mainshock (see, *e.g.*, Ref.[2]). However, this is not the case here.

In order to further clarify the relation with the Omori law, we show in Fig.17 the time dependence of the frequency of aftershocks after the mainshock on a double-logarithmic scale: In the upper panel, the data with the distance range  $r_{max} = 30$  km are shown with varying the magnitude threshold as  $m_c = 3, 4$  and  $5$ , while, in the lower panel, the data with  $m_c = 5$  are shown with varying the distance range as  $r_{max} = 5, 30$  and  $300$  km. In all cases analyzed, a straight-line behavior corresponding to the power-law decay is observed (Omori law). In contrast to the corresponding quantity before the mainshock, the slope of the straight line, *i.e.*,

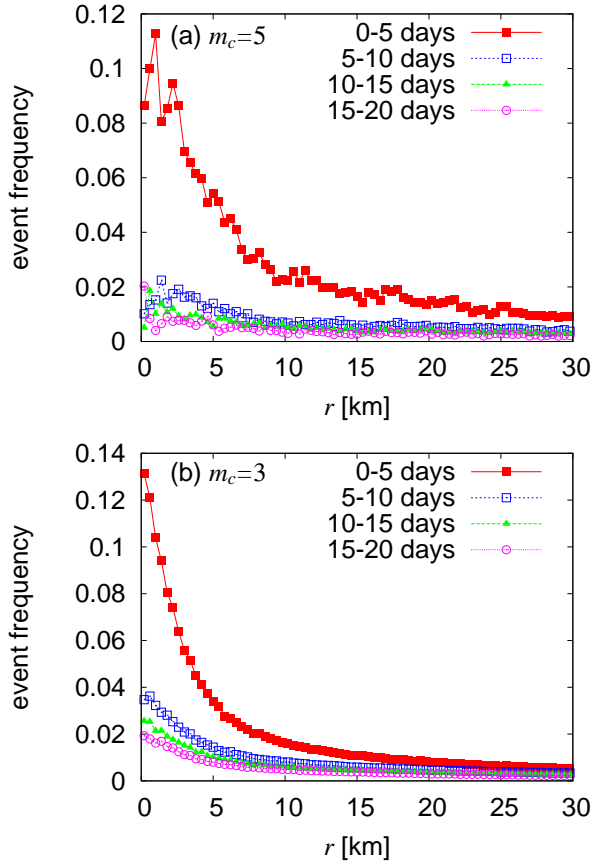


Figure 16: The time evolution of the event frequency of arbitrary magnitude after the mainshock, plotted versus the distance from the epicenter of the mainshock. The magnitude threshold for the mainshock is  $m_c = 5$  (a), and  $m_c = 3$  (b). The data are generated from the JUNE catalog.

the value of the Omori exponent, seems to depend on the distance range  $r_{max}$  and the magnitude of the mainshock  $m_c$ . As the distance range  $r_{max}$  gets smaller and the magnitude of the mainshock  $m_c$  gets larger, the Omori exponent tends to get larger. If one looks at the range  $r_{max} = 5$  km for mainshocks greater than  $m_c = 5$ , the Omori exponent is about 0.71.

The corresponding spatiotemporal correlations after the mainshock are calculated for the 1D BK model, and the results are shown in Fig.18 for the cases of  $\alpha = 1$ . As can be seen from the figure, aftershock activity is clearly observed with the maximum rate occurring at the epicenter of the mainshock. In contrast to the JUNE data, the  $r$ -dependence of the spatial seismic distribution is non-monotonic, aftershock activity being suppressed in the surrounding region where the rupture was largest in the mainshock. The seismicity near the epicenter is kept almost constant

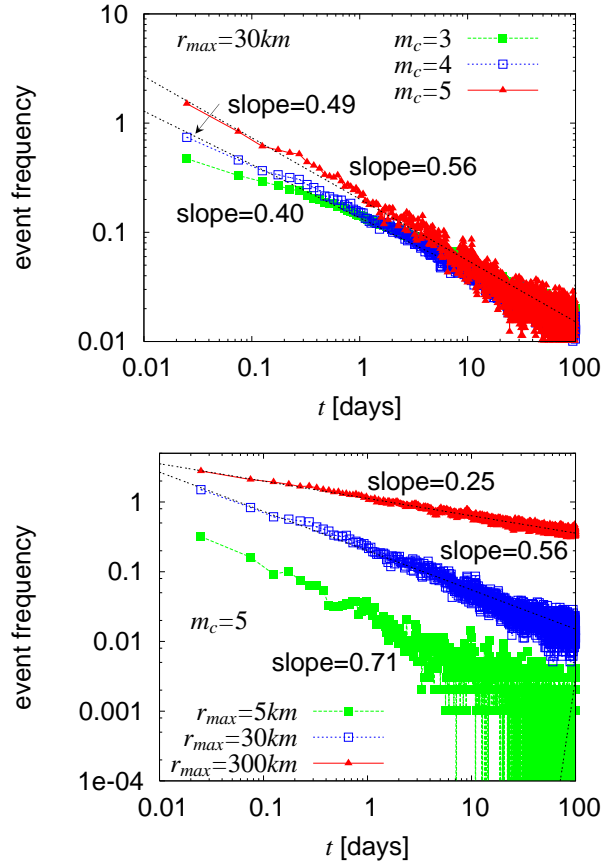


Figure 17: The frequency of seismic events of arbitrary magnitude after the mainshock, plotted versus the time after the mainshock on a double-logarithmic scale. The data are generated from the JUNE catalog. In the upper figure, the magnitude threshold of the mainshock is varied as  $m_c = 3, 4$  and  $5$  with fixing the distance range of observation  $r_{max} = 30$  km, whereas, in the lower figure, the distance range of observation is varied as  $r_{max} = 5, 30$  and  $300$  km with fixing the magnitude threshold  $m_c = 5$ .

in time for some period after the mainshock, say, in the time range  $t\nu < 0.03$ , which is in apparent contrast to the power-law decay as expected from the Omori law: See the insets of Fig.18. At longer time scales, the seismicity near the epicenter seems to decay gradually, although the decay observed here is not a power-law decay. A very much similar behavior is observed also for the 2D BK model: See Fig.19. Hence, aftershocks obeying the Omori law is not realized in the BK model, as already reported [20]. This is in apparent contrast to the observation for real faults.

Such an absence of aftershocks in the BK model might give a hint to the physical origin of aftershocks obeying the Omori law, *e.g.*, they may be driven by the slow chemical process at the fault,

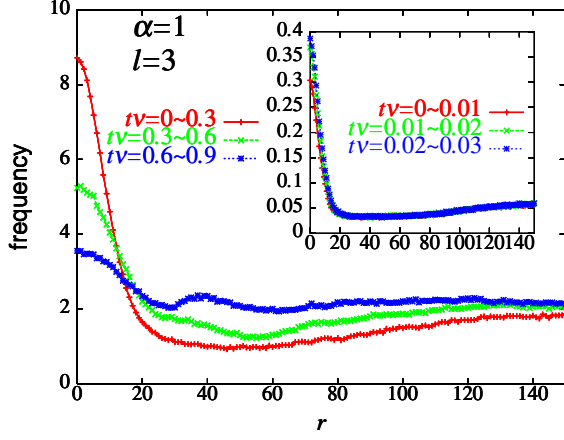


Figure 18: The time evolution of the spatial seismic distribution function after the mainshock of  $\mu > \mu_c = 3$ , calculated for the 1D BK model. The inset represents a similar plot with longer time intervals.

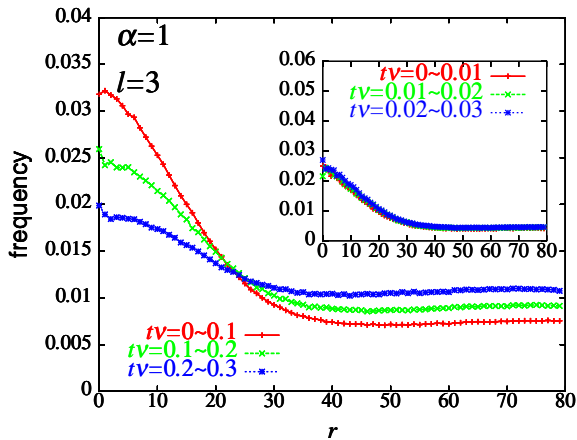


Figure 19: The time evolution of the spatial seismic distribution function after the mainshock of  $\mu > \mu_c = 5$ , calculated for the 2D BK model. The inset represents a similar plot with longer time intervals.

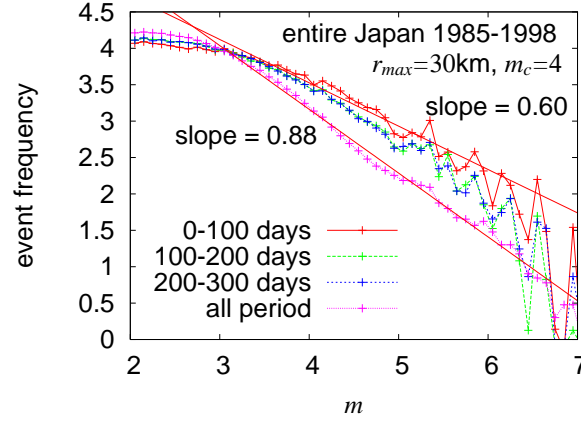


Figure 20: The time-resolved local magnitude distribution of earthquakes in Japan before the mainshock of  $m > m_c = 4$ , generated from the JUNEC catalog. Preceding the mainshock, the  $b$ -value decreases considerably from the long-time average value.

or by the elastoplasticity associated with the ascenosphere, *etc*, which are not taken into account in the BK model.

### 3.6 The time-dependent magnitude distribution

As an other signature of precursory phenomena, we examine a “time-resolved” local magnitude distribution for several time periods before the large event. Fig.20 represents such a local magnitude distribution before large earthquakes, calculated from the JUNEC catalog, *i.e.*, the distribution of seismicity in the vicinity  $r_{max} = 30$  km of the epicenter of the mainshock with its magnitude greater than  $m_c = 4$ . It can clearly be seen from the figure that the GR law persists even just before the mainshock, whereas, preceding the mainshock, the GR exponent  $b$  gets smaller compared with the space- and time-averaged  $b$ -value. For example, 100 days before the mainshock, the  $b$ -value becomes about 0.60, considerably smaller than the averaged value  $b \simeq 0.88$ . Such a decrease of the  $b$ -value was also reported in the literature [49, 50].

For comparison, we show the corresponding local magnitude distributions before the mainshock of the BK models both in 1D (Fig.21) and in 2D (Fig.22). The parameter  $\alpha$  is taken to be  $\alpha = 1$ . In 1D, only events with their epicenters within 30 blocks from the epicenter of the upcoming mainshock are counted, while, in 2D, only events with their epicenters lying in a circle of its radius 5 blocks centered at the epicenter of the upcoming mainshock are counted. As can be seen from the figures, as the mainshock approaches, the form of

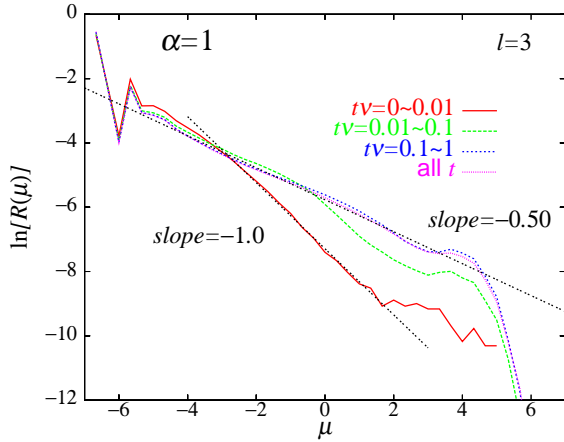


Figure 21: The time-resolved local magnitude distribution of the 1D BK model before the mainshock of  $\mu > \mu_c = 3$ .

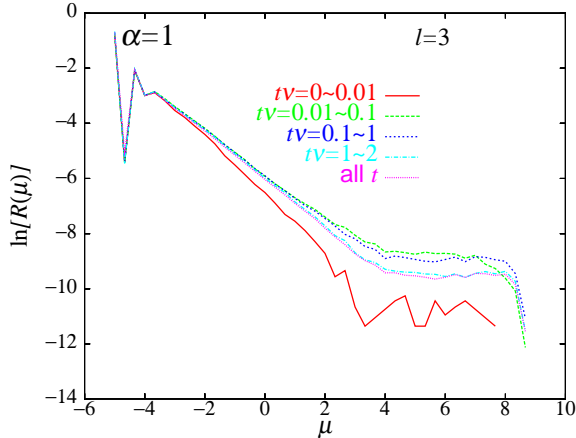


Figure 22: The time-resolved local magnitude distribution of the 2D BK model before the mainshock of  $\mu > \mu_c = 5$ .

the magnitude distribution changes significantly. In 1D, the apparent  $B$ -value describing the power-law regime tends to *increase* as the mainshock approaches, from the time-averaged value  $B \simeq 0.50$  ( $b \simeq 0.75$ ) to the value  $B \simeq 1.0$  ( $b \simeq 1.5$ ) just before the mainshock: It is almost doubled. This tendency is opposite to what we have just found for the JUNEK catalog and several other observations for real faults [49, 50]. However, a similar increase of the apparent  $B$ -value preceding the mainshock was reported for some of real faults [51]. For the case of larger  $\alpha > 1$  (the data not shown here), the change of the  $B$ -value preceding the mainshock is still appreciable, though in a less pronounced manner. More complicated behavior is observed in 2D. As the mainshock approaches, the apparent  $B$ -value describing the power-law

regime *slightly increases first, and then, increases* just before the mainshock.

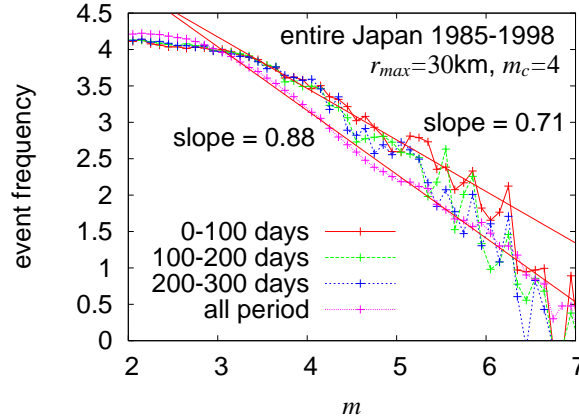


Figure 23: The time-resolved local magnitude distribution of earthquakes in Japan after the mainshock of  $m > m_c = 4$ , generated from the JUNEK catalog.

Next, we analyze similar time-resolved local magnitude distributions, but *after* the large event. Fig.23 represents such a local magnitude distribution after the large event calculated from the JUNEK catalog. In this case, the deviation from the averaged distribution is relatively small as compared with the one observed before the mainshock, although there seems to be a tendency that the observed  $b$ -value decreases slightly after the mainshock.

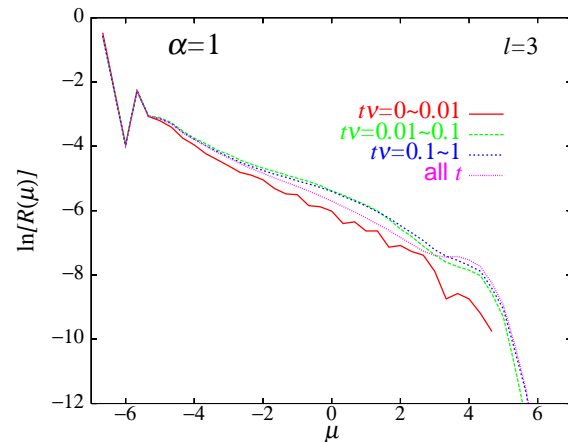


Figure 24: The time-resolved local magnitude distribution of the 1D BK model after the mainshock of  $\mu > \mu_c = 3$ .

For comparison, we show the corresponding local magnitude distributions after the mainshock for the BK models in 1D (Fig.24) and in 2D (Fig.25). The parameter  $\alpha$  is taken to be  $\alpha = 1$ .



As can be seen from the figures, the form of the magnitude distribution changes only little after the mainshock except that the weight of large events is decreased appreciably, particularly in 2D.

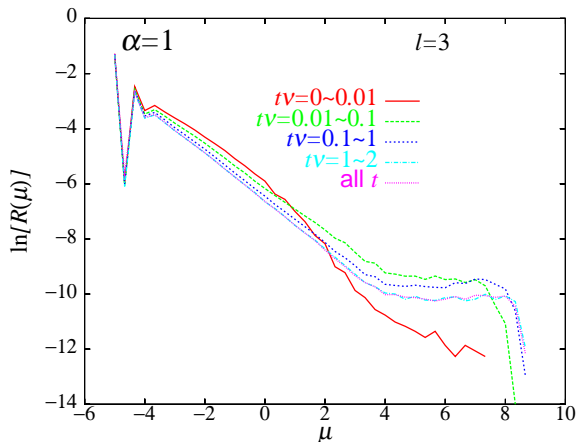


Figure 25: The time-resolved local magnitude distribution of the 2D BK model after the mainshock of  $\mu > \mu_c = 5$ .

## 4 Summary and discussion

In summary, we studied the spatiotemporal correlations of earthquakes both by the analysis of real earthquake catalog of Japan and by numerical computer simulations of the spring-block model in 1D and 2D. Particular attention was paid to the magnitude distribution, the recurrence-time distribution, the time evolution of the spatial distribution of seismicity before and after the mainshock, and the time evolution of the magnitude distribution before and after the mainshock. Certain eminent features of the spatiotemporal correlations, including foreshocks, aftershocks, swarms and doughnut-like seismic pattern, were discussed in some detail.

In our numerical simulations of the BK model, particular attention was paid to the issue how the statistical properties of earthquakes depend on the frictional properties of earthquake faults. We have found that when the extent of the velocity-weakening property is suppressed, the system tends to be more critical, while, as the velocity-weakening property is enhanced, the system tends to be more off-critical with enhanced features of characteristic earthquakes.

Overall, the BK model tends to exhibit more characteristic or off-critical statistical properties, particularly for large earthquakes, than the real seismicity which exhibits much more critical statistical properties. This discrepancy between the

model and the real seismicity has been recognized for some time now, but its true cause has remained to be unclear.

First, we need to recognize that the earthquake catalog is taken not for a single fault, but over many faults. There exists a suspicion that, even if the property of a single individual fault is more or less characteristic the property obtained after averaging over many faults each of which has different characteristics, becomes apparently characteristic as a whole. If this is really the case, the real observation is not necessarily inconsistent with the observation for the BK model, since the BK model deals with the property of a single uniform fault. There is a claim that the extent of the criticality of earthquakes might depend on the type of earthquake faults, *i.e.*, a matured fault with relatively regular fault zone behaves more characteristic, while an immatured fault with relatively irregular fault zone behaves more critical [52]. Difficulty in testing such a hypothesis is that the statistical accuracy of events for a single fault is rather limited, particularly for large events. We need to be careful because, when the event number is not sufficient, an apparent deviation from the criticality might well arise simply due to the insufficient statistics, pretending a characteristic earthquake.

Other possibility is that, since smaller earthquakes are more or less critical even in the BK model, in real seismicity, the critical behavior might be limited to moderately large earthquakes which are contained in enough number in the earthquake catalog, while very large earthquakes, which are very few in number in the catalog, might be more or less characteristic. Anyway, the question of either critical or characteristic earthquakes is one of major fundamental questions left in earthquake studies.

The BK model was found to exhibit several intriguing precursory phenomena associated with large events: Preceding the mainshock, the frequency of smaller events is gradually enhanced, whereas just before the mainshock it is suppressed only in a close vicinity of the epicenter of the upcoming mainshock (the Mogi doughnut). The apparent  $B$ -value of the magnitude distribution increases significantly preceding the mainshock. On the other hand, the Omori law of aftershocks is not observed in the BK model.

Some of these precursory phenomena observed in the BK model are also observed in real earthquake catalog, but some of them are not. For example, the enhancement of foreshock activity is observed in common both in the BK model and in the JUNEK catalog. By contrast, the doughnut-like quiescence generically observed in the BK

model is not observed in standard earthquakes in the JUNEC catalog, although it is observed in certain earthquake swarms.

Here, in order to make a further link between the BK model and the real world, it might be of some interest to estimate various time and length scales involved in the BK model. For this, we need to estimate the units of time and length of the BK model in terms of real-world earthquakes. Concerning the time unit  $\omega^{-1}$ , we estimate it via the rise time of large earthquakes,  $\sim \pi/\omega$ , which is typically about 10 seconds. This gives an estimate of  $\omega^{-1} \sim 3$  sec. Concerning the length unit  $L$ , we estimate it making use of the fact that the typical displacement in large events of our simulation is of order one  $L$  unit, which in real-world large earthquakes is typically 5 meters. Then, we get  $L \sim 5$  meters. Since the loading rate  $\nu'$  associated with the real plate motion is typically 5 cm/year, the dimensionless loading rate  $\nu = N/(L\omega)$  is estimated to be  $\nu \sim 10^{-9}$ . If we remember that the typical mean recurrence time of large events in our simulation is about one unit of  $\nu^{-1}$ , the mean recurrence time of our simulation corresponds to 100 years in real world.

In our simulation of the BK model, the doughnut-like quiescence was observed before the mainshock at the time scale of, say,  $t\nu \lesssim 10^{-2}$ . This time scale corresponds to about 1 year. In our simulation, the doughnut-like quiescence was observed in the region only within a few blocks from the epicenter of the mainshock. To give the corresponding real-world estimate, we need the real-world estimate of our block size  $a$ . In the BK model, the length scale  $a$  is entirely independent of the length scale  $L$ , and has to be determined independently. We estimate  $a$  via the typical velocity of the rupture propagation,  $l\omega$ , which is about 3 km/sec in real earthquakes. From this relation, we get  $a \sim 3$  km. The length scale associated with the doughnut-like quiescence is then estimated to be 3~6 km in radius. If we remember that the rupture size of large events in our simulation with  $\mu = \mu_c = 3$  was about 60 blocks, the size of the rupture size of large earthquakes of our simulation corresponds to 180 km and more. This is comparable to the size of the rupture zone of real earthquakes of their magnitude eight. Hence, the large events in the BK model might correspond to exceptionally large earthquakes in real seismicity, which might explain the reason, at least partially, why the deviation from the GR law observed in the BK model at larger magnitudes is hardly observed in real seismicity. In real faults, the possible maximum size of the rupture zone might be limited by the fault geometry, *i.e.*, by the boundary of a

fault.

Of course, it is not a trivial matter at all how faithfully the statistical properties as observed for the BK model represent those of real earthquakes. We should be careful not to put too much meaning to the quantitative estimates given above.

As an other precursory effect, the change of the apparent  $B$ -value is observed in the BK model, *i.e.*, an increase in 1D or an initial decrease followed by a subsequent increase in 2D. In the JUNEC catalog, the  $B$ -value turns out to decrease prior to the mainshock consistently with several other observations for real faults. Meanwhile, an increase of the  $B$ -value, which is similar to the one observed in the 1D BK model, was reported in some real faults. Thus, to elucidate the detailed mechanism behind the change of the  $B$ -value preceding the large event is an interesting open question.

One thing seems to be clear: Much needs to be done before we understand the true nature of earthquakes. We hope that further progress in statistical-physical approach to earthquakes, combined with the ones in other types of approaches from various branches of science, would eventually promote our fuller understanding of earthquakes.

The author is thankful to Mr. T. Mori and Mr. A. Ohmura for their collaboration and discussion. He is also thankful to Prof. B. Chakrabarti for organizing the MOE conference and for giving me an opportunity of presenting a talk there and writing this article.

## References

- [1] C.H. Scholz, *Nature* **391**, 3411 (1998).
- [2] C.H. Scholz, *The Mechanics of Earthquakes and Faulting* (Cambridge Univ. Press, 1990).
- [3] P. Bak, C. Tang and K. Wiesenfeld, *Phys. Rev. Lett.* **59**, 381 (1987).
- [4] P. Bak and C. Tang, *J. Geophys. Res.* **94**, 15635 (1989).
- [5] R. Burridge and L. Knopoff, *Bull. Seismol. Soc. Am.* **57** (1967) 3411.
- [6] T. Mori and H. Kawamura, *Phys. Rev. Lett.* **94**, 058501 (2005).
- [7] T. Mori and H. Kawamura, *J. Geophys. Res.*, in press (physics/0504218).
- [8] T. Mori and H. Kawamura, unpublished.
- [9] H. Kawamura and T. Mori, unpublished.

- [10] J.M. Carlson, J.S. Langer, B.E. Shaw and C. Tang, Phys. Rev. A**44**, 884 (1991).
- [11] J.M. Carlson, J.S. Langer and B.E. Shaw, Rev. Mod. Phys. **66**, 657 (1994).
- [12] B.E. Shaw, J. Geophys. Res. **100**, 18239 (1995).
- [13] C.R. Myers, B.E. Shaw and J.S. Langer, Phys. Rev. Lett. **77**, 972 (1996).
- [14] J. Dietrich, J. Geophys. Res. **84**, 2161 (1979).
- [15] A. Ruina, J. Geophys. Res. **88**, 10359 (1983).
- [16] S.T. Tse and J.R. Rice, J. Geophys. Res. **91**, 9452 (1986).
- [17] N. Kato, J. Geophys. Res. **109**, B12306 (2004).
- [18] A. Ohmura and H. Kawamura, unpublished.
- [19] J.M. Carlson, Phys. Rev. A**44**, 6226 (1991).
- [20] J.M. Carlson and J.S. Langer, Phys. Rev. Lett. **62**, 2632 (1989); Phys. Rev. A**40**, 6470 (1989).
- [21] J.M. Carlson, J. Geophys. Res. **96**, 4255 (1991).
- [22] J. Schmittbuhl, J.-P. Vilotte and S. Roux, J. Geophys. Res. **101**, 27741 (1996).
- [23] B.E. Shaw, J.M. Carlson and J.S. Langer, J. Geophys. Res. **97**, 479 (1992).
- [24] C.R. Myers and J.S. Langer Phys. Rev. E**47**, 3048 (1993).
- [25] B.E. Shaw, Geophys. Res. Lett. **21**, 1983 (1994).
- [26] R. De and G. Ananthakrisna, Europhys. Lett. **66**, 715 (2004).
- [27] J. Xia, H. Gould, W. Klein and J.B. Rundle, Phys. Rev. Lett. **95**, 248501 (2005); cond-mat/0601679.
- [28] H. Nakanishi, Phys. Rev, A**41**, 7086 (1990).
- [29] K. Ito and M. Matsuzaki, J. Geophys. Res. **95**, 6853 (1990).
- [30] S.R. Brown, C.H. Scholz and J.B. Rundle, Geophys. Res. Lett. **18**, 215 (1991).
- [31] Z. Olami, H.J. Feder and K. Christensen, Phys. Rev, Lett. **68**, 1244 (1992).
- [32] S. Hergarten and H. Neugebauer, Phys. Rev. E**61**, 2382 (2000).
- [33] S. Hainzl, G. Zöller and J. Kurths, J. Geophys. Res. **104**, 7243 (1999); Geophys. Res. Lett. **27**, 597 (2000).
- [34] A. Helmstetter, S. Hergarten and D. Sornette, Phys. Rev, Lett. **88**, 238501 (2002); Phys. Rev. E**70**, 046120 (2004).
- [35] H. Tsuruoka, Abstract of the annual meeting of the Seismological Society of Japan, p04 (1997).
- [36] G.L. Vasconcelos, Phys. Rev. Lett. **76**, 4865 (1996).
- [37] M. S. Vieira, G.L. Vasconcelos and S.R. Nagel, Phys. Rev. E**47**, R2221 (1993).
- [38] I. Clancy and D. Corcoran, Phys. Rev. E**71**, 046124 (2005).
- [39] T.C. Hanks, J. Geophys. Res. **84**, 2235 (1979).
- [40] D.J. Andrews, J. Geophys. Res. **85**, 3867 (1980).
- [41] K. Aki, in *Earthquake Prediction, An International Review*, (ed. D.W. Simpson and P.G. Richards, American Geophysical Union, Washington D.C.) p.566 (1981).
- [42] B.K. Chakarabarti and R.B. Stinchcombe, Physica, A**270**, 27 (1990); P. Bhattacharyya, Physica, A**348**, 199 (2005); P. Bhattacharyya, A. Chatterjee and B.K. Chakarabarti, physics/0510038.
- [43] S.P. Nishenko and R. Buland, Bull. Seismol. Soc. Am. **77**, 1382 (1987).
- [44] P. Bak, K. Christensen, L. Danon and T. Scanlon, Phys. Rev. Lett. **88**, 178501 (2002).
- [45] A. Corral, Phys. Rev. Lett. **92**, 108501 (2004); Phys. Rev. E**68**, 035102 (2003).
- [46] K. Mogi, Bull. Earthquake Res. Inst. Univ. Tokyo **47**, 395 (1969); Pure Appl. Geophys. **117**, 1172 (1979).
- [47] S.L. Pepke, J.M. Carlson and B.E. Shaw, J. Geophys. Res. **99**, 6769 (1994).
- [48] V.G. Kossobokov and J.M. Carlson, J. Geophys. Res. **100**, 6431 (1995).
- [49] S. Suehiro, T. Asada and M. Ohtake, *Papers Meteorol. Geophys.* **15**, 71 (1964).

- [50] S.C. Jaume and L.R. Sykes, *Pure Appl. Geophys.* **155**, 279 (1999).
- [51] W.D. Smith, *Nature* **289**, 136 (1981).
- [52] S.G. Wesnousky, *Nature* **335**, 340 (1988);  
M.W. Stirling, S.G. Wesnousky and K. Shimazaki, *J. Geophys. Res.* **124**, 833 (1996).

